μ Synthesis for a Large Flexible Space Structure Experimental Testbed

B. Boulet[*]
McGill University, Montréal, Québec H3A 2A7, Canada
B. A. Francis[†]
University of Toronto, Toronto, Ontario M5S 1A4, Canada
P. C. Hughes[‡]
University of Toronto, North York, Ontario M3H 5T6, Canada
and
T. Hong[§]
Loki Innovations, Toronto, Ontario M6S 1N9, Canada

An application is presented of μ synthesis to the robust control of a large flexible space structure experimental testbed called Daisy. A perturbed left-coprime factorization of Daisy's dynamics is used to capture the uncertainty in the modes. Designs of the μ synthesis controller based on left-coprime factorizations of 46th-order collocated and noncollocated models of Daisy are presented together with simulation and experimental results. These results are compared to those obtained with $\mathcal{H}_\infty$ controllers, and it is shown that the μ controllers performed better. These controllers provide robust performance with respect to given bounds on modal parameter uncertainties without resorting to computationally complex techniques involving real structured perturbations.

Nomenclature

B_1, C_1	=	input and output matrices of modal model of large flexible space structures (LFSS)
$\mathcal{BRH}_\infty$	=	unit open ball in $\mathcal{RH}_\infty$
D	=	diagonal damping matrix of modal model of LFSS
$D(A_d, T, \text{axes})$	=	double-pulse hub torque disturbance used in simulations and experiments
$\mathcal{D}_r$	=	set of factor perturbations in $\mathcal{RH}_\infty$ with $\|r^{-1}\boldsymbol{\Delta}_0\|_\infty < 1$
d	=	input torque disturbance
e	=	angle errors
$\mathcal{F}_L(P, K)$	=	lower linear fractional transformation of P by K
$\mathcal{F}_U(P, \Delta)$	=	upper linear fractional transformation of P by Δ
G	=	nominal plant model, $:= u \mapsto \eta$
$\mathcal{H}_\infty$	=	Hardy space of functions analytic in $\mathbb{C}_+$ and bounded on the imaginary axis, with norm $\|Q\|_\infty := \sup_{\omega \in \mathbb{R}} \|Q(j\omega)\|$
J_1, J_2	=	diagonal scaling matrices
K, K_i	=	finite-dimensional linear time-invariant multi-input/multi-output controllers, $i = 1, 2, 3$
K_{pid}	=	discretized unscaled controllers designed for Daisy, $i = 1, 2, 3$
$\tilde{M}, \tilde{N}$	=	left-coprime factors of nominal plant factorization
$\tilde{M}_0, \tilde{N}_0$	=	scaled nominal left-coprime factors
m, p, n	=	number of inputs, outputs, and modes in LFSS model
$\|Q\|$	=	spectral norm of Q (maximum singular value)
$\mathbb{R}, \mathbb{C}$	=	real and complex numbers
$\mathcal{RH}_\infty$	=	space of real-rational functions in $\mathcal{H}_\infty$
r	=	input reference
$\boldsymbol{r}$	=	bound on the factor uncertainty ($\boldsymbol{r}, \boldsymbol{r}^{-1}$ in $\mathcal{RH}_\infty$)
S_d	=	sensitivity from d to y
S_{dh}	=	sensitivity from d to y_h
S_{dhp}	=	perturbed sensitivity from d to y_h
$\boldsymbol{T}_a$	=	diagonal transfer matrix of actuator dynamics
u, u_{sc}	=	hub and rib torque input signal, scaled version
$u \mapsto v$	=	transfer matrix from u to v
$\hat{v}$	=	Laplace transform of the signal v
w	=	input signal coming from the perturbation
$\boldsymbol{w}, \boldsymbol{W}$	=	weighting functions for performance
y	=	measured hub and rib angles used for feedback
y_h, y_r	=	hub and rib angles (components of y)
z	=	output signal whose norm is to be minimized
Γ	=	structured uncertainty set
γ, d_{max}	=	scaling factor
Δ_s	=	complex structured perturbation
$\hat{\boldsymbol{\Delta}}_0$	=	scaled factor perturbation normalized by $\boldsymbol{r}$
η	=	modal coordinates of LFSS model
$\theta_{hx}, \theta_{hy}, \theta_{hz}$	=	Daisy's hub angles around the x, y, and z axes
Λ	=	diagonal matrix of squared modal frequencies
$\mu_\Gamma(Q)$	=	structured singular value of Q with respect to set Γ
ω_i, ζ_i	=	natural frequency and damping ratio of ith mode

I. Introduction

IN the near future, large flexible space structures (LFSS) such as space stations or large communication satellites will be used in orbit around the Earth to carry wide antennas, solar panels, scientific instruments, crewed research laboratories, and so on. Because

of their dimensions of up to several hundred meters, LFSS must be assembled in space using lightweight truss assemblies. As a result, these structures are flexible, and their dynamics typically possess several low-damped, clustered low-frequency flexible modes. Experimental testbeds featuring these characteristics have been built,[1] such as Daisy[2] at the University of Toronto Institute for Aerospace Studies (UTIAS).

Dynamic models of LFSS are usually obtained using finite element methods, but these models are known to be reasonably accurate only for a few of the most significant modes of the structure. The uncertainty in the remaining modes of the model, together with the special properties of LFSS dynamics, poses a challenging problem to the control engineer. In this paper, we are concerned with the design and experimental testing of finite-dimensional linear time-invariant controllers achieving robust performance for two models of Daisy using μ synthesis. These collocated and noncollocated models have up to 10% uncertainty in the modal frequencies and 50% in the damping ratios. The noncollocated model represents Daisy with three measured degrees of freedom that are used for feedback but are not actuated. Two μ-synthesis designs based on perturbed left-coprime factorizations (LCFs) of the collocated and noncollocated models of Daisy are presented together with simulation and experimental results. The LCFs were derived following the method developed by the authors in Ref. 3. The results are compared to those obtained with $\mathcal{H}_\infty$ controllers in Ref. 3, and it is shown that the μ controllers performed better.

A. Uncertainty Models for LFSS

Uncertainty modeling in LFSS is critical if one is to achieve acceptable robustness and performance levels with a practical controller. Some works[4–6] use norm-bounded additive or multiplicative perturbations of a nominal model in the frequency domain to account for uncertainty in the modal frequencies, damping ratios, and mode shape matrix of the model. Unmodeled modes of the structure and uncertain actuator dynamics can also be represented in this way.[7] Such approaches to uncertainty modeling in LFSS do not handle modal parameter uncertainty very well: Slight variations in either the mode frequencies or damping ratios usually cause the associated dynamic perturbations to be large in the ∞-norm sense. In Ref. 3, a technique is described where real parameter uncertainty in the modes is transformed into unstructured uncertainty in the factors of an LCF of LFSS dynamics, without introducing too much conservativeness. This is the uncertainty model adopted in this paper. The resulting set of perturbed LCFs is guaranteed to include all perturbed plant models produced by variations in the modal parameters within their bounds. Uncertainty in the nominal factors can also represent unmodeled modes and actuator dynamics.

A frequency-domain representation of the uncertainty is motivated by the fact that many results and practical controller design techniques are available for this kind of uncertainty. On the other hand, a more direct approach would use a real uncertainty model.[4,8–10] However, these methods quickly become numerically difficult as the number of independent scalar perturbations increases.[11] Furthermore, unmodeled modes may cause spillover if only real scalar uncertainty is considered.

Upper and lower linear fractional transformations are now defined. Suppose the matrix P is partitioned as

$$P := \begin{bmatrix} P_{11} & P_{12} \\ P_{21} & P_{22} \end{bmatrix}$$

K is such that its transpose K^T has the same dimensions as P_{22}, and Δ is such that its transpose Δ^T has the same dimensions as P_{11}. Then the lower linear fractional transformation (LFT) of P by K is $\mathcal{F}_L(P, K) := P_{11} + P_{12}K(I - P_{22}K)^{-1}P_{21}$ whenever the inverse exists. The upper LFT of P by Δ is $\mathcal{F}_U(P, \Delta) := P_{22} + P_{21}\Delta(I - P_{11}\Delta)^{-1}P_{12}$ whenever the inverse exists. These definitions, which also hold for system matrices, are best illustrated by the two block diagrams in Fig. 1, where $\mathcal{F}_L(P, K) = u_1 \mapsto v_1$ and $\mathcal{F}_U(P, \Delta) = u_2 \mapsto v_2$.
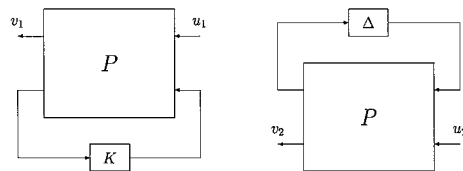

Fig. 1 Lower LFT $\mathcal{F}_L(P, K)$ and upper LFT $\mathcal{F}_U(P, \Delta)$.

B. Performance Objectives

Typical performance objectives for LFSS include tracking of a desired trajectory by the rigid part of the LFSS (slewing maneuver), attitude regulation, and vibration attenuation in the flexible part of the structure. The latter two objectives will be considered for Daisy in this paper. These objectives can be translated into more quantitative performance specifications such as desired shapes of the appropriate closed-loop sensitivity matrices in the frequency domain. Closed-loop performance robustness to perturbations of the modal parameters within their a priori known bounds is guaranteed provided that the so-called μ norm of a certain closed-loop sensitivity matrix can be made less than one with a stabilizing controller.

The robust performance control design problem is formulated as a standard μ synthesis. This design technique has been studied extensively in the past decade, and well-developed algorithmic solutions are available (see Ref. 12 for an introduction to μ synthesis). The MATLAB® μ-Analysis and Synthesis Toolbox (μ-Tools) was used to compute the controllers designed in this paper.

C. Organization

This paper is organized as follows: Section II is a description of Daisy, an LFSS experimental testbed built at UTIAS. The controllers developed in this research were tested and compared on Daisy. Section III reviews an LCF modeling technique for LFSS introduced in Ref. 3 and applies it to Daisy. Section IV briefly reviews the μ-synthesis design technique for robust performance. Collocated and noncollocated controllers are designed for Daisy in Sec. IV using this technique. Details of controller implementation on Daisy and experimental results are also given in Sec. IV. Then Sec. V presents results obtained with $\mathcal{H}_\infty$ controllers and compares them with those obtained with the μ controllers. Conclusions are drawn in Sec. VI.

II. Daisy: LFSS Experimental Testbed

Daisy's dynamics are meant to approximate those of real LFSS (see Fig. 2 and Refs. 2 and 3). It consists of a rigid hub mounted on a spherical joint and on top of which are 10 ribs attached through passive two-degree-of-freedom rotary joints and low-stiffness springs. Each rib is coupled to its two neighbors via low-stiffness springs. The hub represents the rigid part of the LFSS, and the ribs model the flexibilities in the LFSS. Each rib is equipped with two bidirectional air jet thrusters that are essentially on–off devices, each capable of delivering a torque of 0.8 N · m at the rib joint. Pulse-width modulation (PWM) of the thrust is used to apply desired torques on the ribs. The thruster PWM subsystem operates at 10 Hz with duty cycle commands varying from 0 to 100% in both directions.

A digital electrooptic position sensor (DEOPS),[13] consisting of two hub-mounted infrared cameras, measures the positions of infrared emitting diodes mounted at the tip of each rib. The cameras are linked to a computer, which, from the kinematics of Daisy, computes the 20 rib angles relative to the hub in real time (at a 30-Hz sampling rate) from the sampled infrared video frames. DEOPS was developed at UTIAS.[13] Its resolution is approximately 0.1% of the cameras' fields of view, which roughly translates to a rib angle measurement accuracy of 3.5×10^{-4} rad (0.02 deg) in the ideal case. The hub actuators consist of three orthogonal reaction wheels driven by dc motors. Each is limited to a maximum torque of 38.8 N · m. Hub orientation and angular velocity are measured with position and velocity encoders. For this research, only DEOPS and the hub angle encoders were used as sensors.

The original dynamic model for Daisy is of 46th order, including 20 flexible modes with nominal frequencies ranging from approximately 0.56 to 0.71 rad/s and modal damping ratios from 0.015 to 0.06 (Table 1). Some of the modes are multiple. This original

finite-dimensional linear time-invariant dynamic model of Daisy was obtained from an extensive modeling effort of each one of Daisy's mechanical parts during its design phase and using the Newton–Euler method to determine its coupled dynamic equations, which were then linearized. Note that Daisy's dynamics are described by a set of ordinary differential equations rather than partial differential equations. The flexibility is entirely lumped in the springs on the rib joints and those coupling the ribs together.

We conducted open-loop experiments to obtain estimates of bounds on modal parameter uncertainty. Uncertainty in the modal frequencies and damping ratios was estimated to 10 and 50%, respectively. Two of the rigid-body modes are considered as flexible modes because they are pendulous. The nominal dynamic equations in modal coordinates are as follows[3]:

$$\ddot{\eta} + D\dot{\eta} + \Lambda\eta = B_1 u \tag{1}$$

$$y = C_1 \eta \tag{2}$$

where the input vector

$$u := \begin{bmatrix} \tau_h \\ \tau_r \end{bmatrix} \in \mathbb{R}^m$$

Table 1 Modal parameters of Daisy's original and refined models

Mode i	Original model		Refined model
	ω_i, rad/s	ζ_i	ω_i, rad/s
1 (rigid)	0	0	0
2 (rigid)	$0.286 \pm 10\%$	$0.11 \pm 50\%$	$0.31 \pm 5\%$
3 (rigid)	$0.293 \pm 10\%$	$0.09 \pm 50\%$	$0.31 \pm 5\%$
4 (flexible)	$0.568 \pm 10\%$	$0.025 \pm 50\%$	$0.60 \pm 5\%$
5 (flexible)	$0.568 \pm 10\%$	$0.02 \pm 50\%$	$0.59 \pm 5\%$
6 (flexible)	$0.569 \pm 10\%$	$0.03 \pm 50\%$	$0.59 \pm 5\%$
7 (flexible)	$0.569 \pm 10\%$	$0.02 \pm 50\%$	$0.59 \pm 5\%$
8 (flexible)	$0.569 \pm 10\%$	$0.035 \pm 50\%$	$0.62 \pm 5\%$
9 (flexible)	$0.569 \pm 10\%$	$0.025 \pm 50\%$	$0.61 \pm 5\%$
10 (flexible)	$0.569 \pm 10\%$	$0.02 \pm 50\%$	$0.70 \pm 5\%$
11 (flexible)	$0.572 \pm 10\%$	$0.02 \pm 50\%$	$0.76 \pm 5\%$
12 (flexible)	$0.592 \pm 10\%$	$0.06 \pm 50\%$	$0.61 \pm 5\%$
13 (flexible)	$0.593 \pm 10\%$	$0.06 \pm 50\%$	$0.60 \pm 5\%$
14 (flexible)	$0.657 \pm 10\%$	$0.015 \pm 50\%$	$0.78 \pm 5\%$
15 (flexible)	$0.657 \pm 10\%$	$0.015 \pm 50\%$	$0.77 \pm 5\%$
16 (flexible)	$0.657 \pm 10\%$	$0.02 \pm 50\%$	$0.79 \pm 5\%$
17 (flexible)	$0.657 \pm 10\%$	$0.02 \pm 50\%$	$0.70 \pm 5\%$
18 (flexible)	$0.657 \pm 10\%$	$0.027 \pm 50\%$	$0.59 \pm 5\%$
19 (flexible)	$0.657 \pm 10\%$	$0.025 \pm 50\%$	$0.63 \pm 5\%$
20 (flexible)	$0.657 \pm 10\%$	$0.02 \pm 50\%$	$0.61 \pm 5\%$
21 (flexible)	$0.670 \pm 10\%$	$0.04 \pm 50\%$	$0.75 \pm 5\%$
22 (flexible)	$0.672 \pm 10\%$	$0.05 \pm 50\%$	$0.75 \pm 5\%$
23 (flexible)	$0.714 \pm 10\%$	$0.015 \pm 50\%$	$0.79 \pm 5\%$

is composed of torques

$$\tau_h := \begin{bmatrix} \tau_x \\ \tau_y \\ \tau_z \end{bmatrix}$$

applied to the hub around three orthogonal axes, and two torques applied on each rib in the out-of-cone and in-cone directions (Fig. 3) for a total of 20 torques in τ_r for the collocated case. By collocated we mean that all rotations and displacements produced by the actuators at their locations are measured and that each sensor has a corresponding (collocated) actuator. Thus, 23 actuator/sensor pairs are used, namely, the 20 bidirectional rib thrusters with the DEOPS system measuring the 20 rib angles, plus the three hub reaction wheels with the three corresponding angle encoders. The output vector

$$y := \begin{bmatrix} y_h \\ y_r \end{bmatrix}$$

is partitioned accordingly. The matrices in Eqs. (1) and (2) are defined as follows: $D := \mathrm{diag}\{0, 2\zeta_2\omega_2, \ldots, 2\zeta_{23}\omega_{23}\}$, $\Lambda := \mathrm{diag}\{0, \omega_2^2, \ldots, \omega_{23}^2\}$, $B_1 \in \mathbb{R}^{23 \times m}$, and $C_1 \in \mathbb{R}^{23 \times 23}$. The number of inputs m is 23 for the collocated model and 20 for the noncollocated model.

Taking the Laplace transform on both sides of Eqs. (1) and (2) with zero initial conditions, we obtain

$$\hat{\eta}(s) = [s^2 I + sD + \Lambda]^{-1} B_1 \hat{u}(s) \tag{3}$$

$$\hat{y}(s) = C_1 [s^2 I + sD + \Lambda]^{-1} B_1 \hat{u}(s) \tag{4}$$

Note that Daisy is not easy to control: Collocated $\mathcal{H}_2$ controllers designed without robustness considerations and implemented on Daisy failed to stabilize it.

III. LCF for Daisy

The use of coprime factorizations to model LFSS dynamics offers the control designer the advantage of having to deal with only one full uncertainty block in the frequency domain. The uncertainty in the coprime factors can account for both modal parameter uncertainty and unmodeled dynamics. With this uncertainty model, standard $\mathcal{H}_\infty$ and μ-synthesis controller design techniques can be used to design for robust stability or robust performance with guaranteed stability or performance margins with respect to variations in the modal parameters. This paper focuses on μ synthesis for Daisy.

In this section, a brief review of the LCF modeling technique for LFSS introduced in Ref. 3 is presented. Consider the matrix $[s^2 I + sD + \Lambda]$ in Eq. (3). It is diagonal, and so its inverse is simply
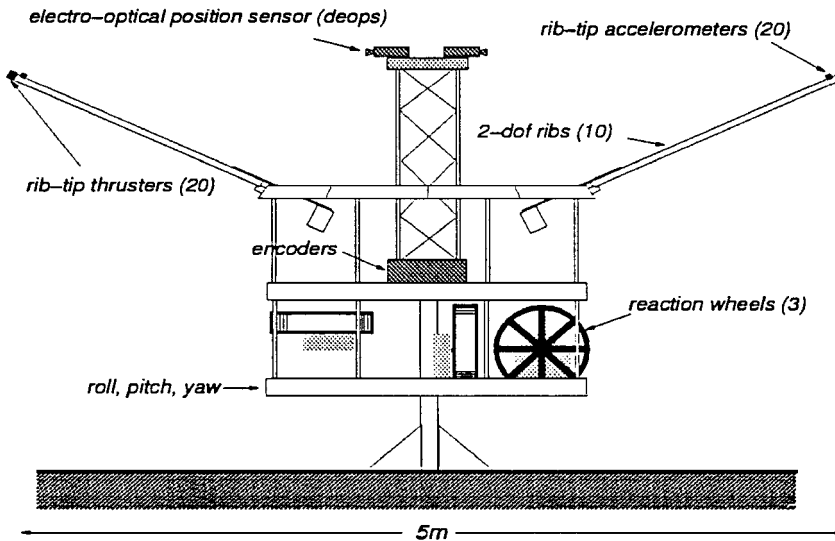

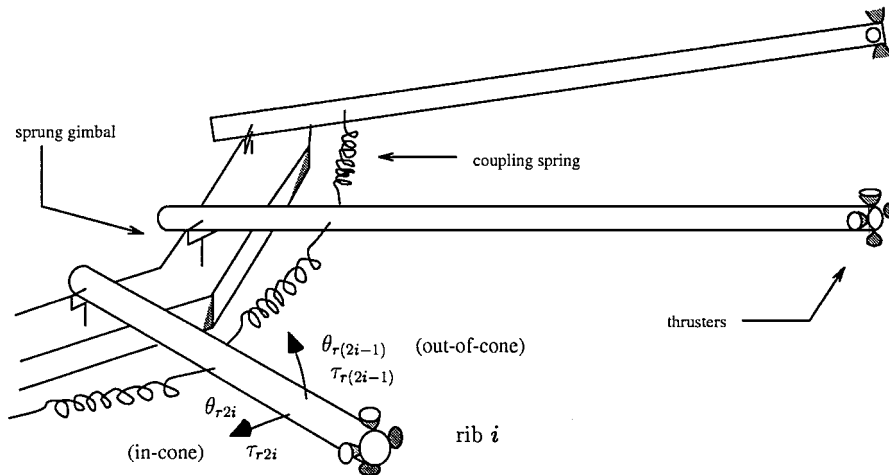Fig. 2   Daisy LFSS experimental testbed.

Fig. 3   Details of Daisy's ribs.

$$[s^2 I + sD + \Lambda]^{-1}$$

$$= \mathrm{diag}\left\{\frac{1}{s^2}, \frac{1}{s^2 + 2\zeta_2\omega_2 s + \omega_2^2}, \ldots, \frac{1}{s^2 + 2\zeta_{23}\omega_{23}s + \omega_{23}^2}\right\} \quad (5)$$

Let the polynomial $s^2 + as + b$ be Hurwitz with real zeros. Form the matrices $\tilde{M}(s)$ and $\tilde{N}(s)$ as follows:

$$\tilde{M}(s) := [1/(s^2 + as + b)]$$

$$\times \mathrm{diag}\left\{s^2, s^2 + 2\zeta_2\omega_2 s + \omega_2^2, \ldots, s^2 + 2\zeta_2\omega_2 s + \omega_2^2\right\} \quad (6)$$

$$\tilde{N}(s) := [1/(s^2 + as + b)]B_1 \quad (7)$$

In our notation, boldface is used for transfer functions and transfer matrices, lower case for signals, scalar constants, and transfer functions, and upper case for constant matrices and transfer matrices. The complex argument s is dropped hereafter to ease the notation. Note that $\tilde{M}$ and $\tilde{N}$ are stable and proper; hence, they belong to $\mathcal{RH}_\infty$. Let the transfer function matrix from $\hat{u}$ to $\hat{\eta}$ be denoted as G. Then G can be written as $\tilde{M}^{-1}\tilde{N}$, that is, $\tilde{M}$ and $\tilde{N}$ form a left factorization of G in $\mathcal{RH}_\infty$. It is easy to show that this factorization is in fact left coprime.[14] Balancing and scaling the factors as explained in Ref. 3, one obtains the scaled left-coprime factors $\tilde{M}_0$ and $\tilde{N}_0$.

A scalar first-order weighting function r bounding the norm of the scaled factor perturbations induced by real parameters was also derived in Ref. 3. Let ΔN_0 and $\Delta M_0 \in \mathcal{RH}_\infty$ be general additive perturbations of the factors $\tilde{N}_0$ and $\tilde{M}_0$, respectively. Define the uncertainty matrix $\mathbf{\Delta}_0 := [\Delta N_0 \; -\Delta M_0]$, and the uncertainty set

$$\mathcal{D}_r := \left\{\mathbf{\Delta}_0 \in \mathcal{RH}_\infty : \left\|r^{-1}\mathbf{\Delta}_0\right\|_\infty < 1\right\} \quad (8)$$

where r and $r^{-1} \in \mathcal{RH}_\infty$.

The weighting function r has the important property that the corresponding family of perturbed plant models contains all models induced by variations in the modal parameters within some a priori known bounds. For example, our collocated model of Daisy has roughly 10% uncertainty in the modal frequencies and 50% in the modal damping ratios. Let G_{rp} denote the transfer matrix mapping u to η when the modal parameters are perturbed within these bounds. When Proposition 1 in Ref. 3 and the modal parameters listed in Table 1 are used, the following weighting function is computed:

$$r(s) = \frac{0.001s + 1.415}{2.33s + 1} \quad (9)$$

Then any transfer matrix model G_{rp} for Daisy can be represented by a transfer matrix in the set $\mathcal{P}$:

$$G_{rp} \in \mathcal{P} := \left\{(\gamma/d_{\max})J_1(\tilde{M}_0 + \Delta\tilde{M}_0)^{-1}(\tilde{N}_0 + \Delta N_0)J_2 : \mathbf{\Delta}_0 \in \mathcal{D}_r\right\} \quad (10)$$
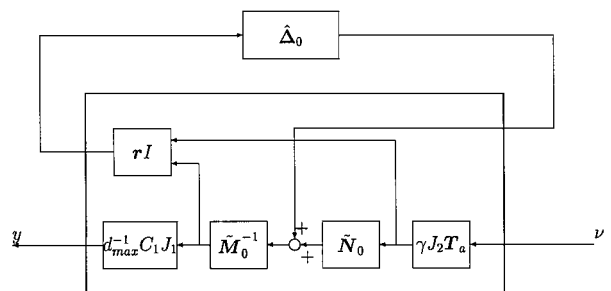

Fig. 4   Perturbed factorization of Daisy's dynamics after scaling.

where γ and $d_{\max}$ are scaling factors and J_1, J_2 are diagonal real scaling matrices computed from the modal uncertainty bounds in Table 1 (see Ref. 3). Note that r is not too conservative in the sense that it tightly covers the worst-case factor perturbation induced by variations in the modal parameters. This is not to say that at each frequency the set of full complex perturbations bounded by $|r(j\omega)|$ is a geometrically tight cover for modal parameter uncertainties, which it is not.

Figure 4 shows the perturbed model for Daisy including the nominal coprime factors, the normalized factor perturbation $\hat{\mathbf{\Delta}}_0 \in \mathcal{BRH}_\infty^{m \times (m+n)}$, the output matrix C_1, the diagonal input and output scaling matrices J_1 and J_2 and scalars γ and $d_{\max}$, and a diagonal matrix of actuator dynamics T_a. Note that $\mathbf{\Delta}_0 = r\hat{\mathbf{\Delta}}_0$ is an arbitrary element in $\mathcal{D}_r$. In this way, r can be included separately in the block diagram of Fig. 4. For the actuator transfer matrix, we define the torque command ν whose Laplace transform is related to the Laplace transform of the actual input torque by $\hat{u} = T_a\hat{\nu}$. The scaling matrices and scalars are important (see Ref. 3 for details on how they are computed) for the inputs and outputs to have the same order of magnitude, which reduces conservativeness of the bounding function r.

IV. μ Synthesis for Daisy

The setup for a μ synthesis is shown in Fig. 5. It includes the scaled and normalized LCF of Fig. 4, together with the hub and rib angle reference inputs $r \in \mathbb{R}^{23}$ and torque disturbance inputs $d \in \mathbb{R}^m$, which are collocated with the actuator torques. Note that the dashed line for the reference signal means that it is not included in the design. The input signal u_{sc} is just a scaled version of the physical torque command ν: $u_{sc} := (\gamma/d_{\max})J_2\nu$. Note that the scaling factors γ, $d_{\max}$, and J_2 are lumped into the controller K. A torque disturbance rejection performance requirement is explicitly introduced in the design by the mapping $d \mapsto z_2$, whose ∞ norm is to be reduced to a value no greater than one. The operator $d \mapsto z_2$ is just the transfer matrix (or sensitivity) mapping the torque disturbance d to the hub angles y_h, weighted by the function $W := w[I_3 \; 0_{3 \times 20}]$, where w is taken to be a high-gain second-order low-pass filter.

More specifically, we want to shape the closed-loop sensitivity $S_{dh} := d \mapsto y_h$, that is, we want to achieve a low sensitivity at low frequencies: $\|S_{dh}(j\omega)\| \leq |w^{-1}(j\omega)|$, $\forall\omega$. However, we require that this inequality hold (and internal stability, too) for all perturbations of the modal parameters and entries of B_1 within their ranges ($\pm 8\%$ of their nominal values for the collocated model and $\pm 5\%$ for the refined noncollocated model). Thus, we require that, for every $\hat{\Delta}_0 \in \mathcal{BRH}_\infty$, the perturbed sensitivity matrix $S_{dhp} := d \mapsto z_2 = \mathcal{F}_L[\mathcal{F}_U(P, \hat{\Delta}_0), K]$, where the LFTs are constructed according to Fig. 5, has its ∞ norm less than or equal to one. This is a robust performance requirement well suited for μ synthesis.

Recall that, for a block structure $\Gamma \subset \mathbb{C}^{n \times n}$ and a matrix $M \in \mathbb{C}^{n \times n}$, the structured singular value $\mu_\Gamma(M)$ is defined as follows:

$$\mu_\Gamma(M) := [\min\{\|\Delta_s\| : \Delta_s \in \Gamma, \det(I - M\Delta_s) = 0\}]^{-1} \quad (11)$$

unless no $\Delta_s \in \Gamma$ makes $I - M\Delta_s$ singular, in which case $\mu_\Gamma(M) := 0$.

Thus, $\mu_\Gamma(M)$ is the reciprocal of the norm of the smallest structured perturbation, $\Delta_s \in \Gamma$, that causes instability of a feedback interconnection of Δ_s and M, in the sense of singularity of the matrix $I - M\Delta_s$.

Consider the perturbed closed-loop system in Fig. 5, where $z_2(t) \in \mathbb{R}^{n_{z_2}}$ and $d(t) \in \mathbb{R}^{n_d}$. The generalized plant P with inputs w, d, and u_{sc} and outputs z_1, z_2, and y is given by
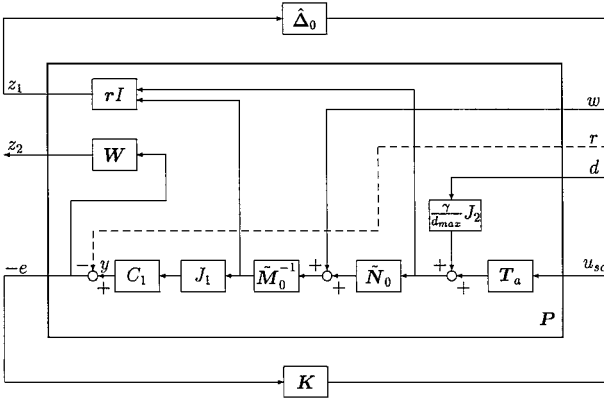
$$P := \begin{bmatrix} P_{11} & P_{12} & P_{13} \\ P_{21} & P_{22} & P_{23} \\ P_{31} & P_{32} & P_{33} \end{bmatrix} \quad (12)$$

where

$$P_{11} := \begin{bmatrix} 0 \\ r\tilde{M}_0^{-1} \end{bmatrix}, \qquad P_{12} := \frac{\gamma}{d_{\max}} \begin{bmatrix} rJ_2 \\ r\tilde{M}_0^{-1}\tilde{N}_0 J_2 \end{bmatrix}$$

$$P_{13} := \begin{bmatrix} r T_a \\ r\tilde{M}_0^{-1}\tilde{N}_0 T_a \end{bmatrix}, \qquad P_{21} := W_1 C_1 J_1 \tilde{M}_0^{-1}$$

$$P_{22} := \frac{\gamma}{d_{\max}} W_1 C_1 J_1 \tilde{M}_0^{-1} \tilde{N}_0 J_2, \qquad P_{23} := W_1 C_1 J_1 \tilde{M}_0^{-1} \tilde{N}_0 T_a$$

$$P_{31} := C_1 J_1 \tilde{M}_0^{-1}, \qquad P_{32} := \frac{\gamma}{d_{\max}} C_1 J_1 \tilde{M}_0^{-1} \tilde{N}_0 J_2$$

$$P_{33} := C_1 J_1 \tilde{M}_0^{-1} \tilde{N}_0 T_a$$

From the so-called small-μ theorem,[12] the key idea for designing controllers achieving robust performance is to introduce a fictitious perturbation Δ_p that wraps as a feedback around the generalized plant, with input z_2 and output d in our current setting (Fig. 5). Then, the robust performance problem is turned into a robust stability
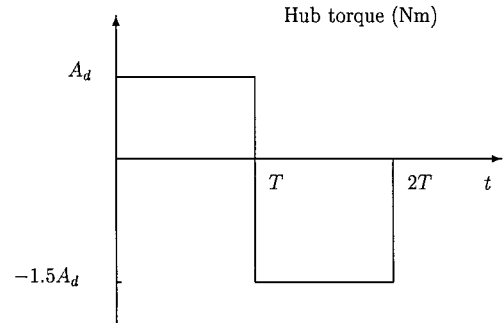

Fig. 5 Generalized plant with scaled perturbation and controller for μ synthesis.

Fig. 7 Standard hub torque disturbance D (A_d, T, axes).

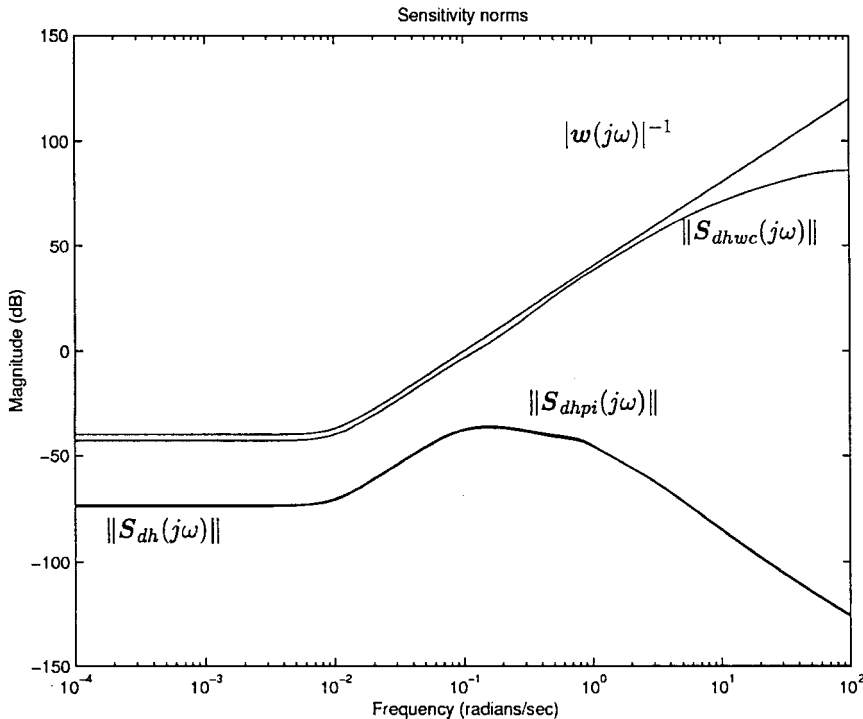**Fig. 6 Norms of $S_{dh}(j\omega)$, $S_{dhwc}(j\omega)$, and $S_{dhp_i}(j\omega)$ for K_1.**

problem for the new system with $\boldsymbol{\Delta}_p$. Let us formalize this for our problem. Consider the system in Fig. 5 and define the following complex structured uncertainty set:

$$\Gamma := \left\{ \begin{bmatrix} \hat{\Delta}_0 & 0 \\ 0 & \Delta_p \end{bmatrix} : \hat{\Delta}_0 \in \mathbb{C}^{23 \times (m+23)}, \Delta_p \in \mathbb{C}^{m \times 3} \right\} \quad (13)$$

Let $\mu_\Gamma: \mathbb{C}^{(m+26) \times (m+23)} \to \mathbb{R}_+$ be the structured singular value associated with the structured perturbations in Γ. From a computational standpoint, $\mu_\Gamma(M)$ can be computed to any desired accuracy because there are only two full blocks in Γ (Ref. 15): one for the coprime factor uncertainty and a fictitious one for the performance specification.

When the small-μ theorem is used, it is easy to prove the following, which is a condition for a stabilizing controller K to achieve robust performance, that is, $\|(WS_{dhp})(j\omega)\| \leq 1, \forall \omega, \forall \hat{\Delta}_0 \in \mathcal{BRH}_\infty$.

Theorem 1: Assume K is internally stabilizing for the nominal plant P. Then for the system in Fig. 5, $\forall \hat{\Delta}_0 \in \mathcal{BRH}_\infty$, the closed loop is well posed, internally stable, and $\|d \mapsto z_2\|_\infty \leq 1$ iff $\sup_{\omega \in \mathbb{R}} \mu_\Gamma\{\mathcal{F}_L[P(j\omega), K(j\omega)]\} \leq 1$.

Thus, a μ synthesis can be performed on the generalized plant P. That is, we can implement a standard D–K iteration algorithm[12] to minimize $\sup_{\omega \in \mathbb{R}} \mu_\Gamma\{\mathcal{F}_L[P(j\omega), K(j\omega)]\}$.

A. Controller Design: Collocated Case

It is desired to control Daisy so that it remains stable and achieves the desired torque disturbance rejection level $\|S_{dhp}(j\omega)\| \leq |w^{-1}(j\omega)|, \forall \omega$, for all bounded perturbations of the modal parameters in Table 1 and all perturbations of the entries of B_1 within 8% of their nominal values. The diagonal scaling matrices J_1 and J_2 are computed as explained in Ref. 3. The generalized plant for μ synthesis is built according to Eq. (12), and the constants and weighting functions are

$$d_{\max} = 0.107, \qquad \gamma = 0.79$$

$$w(s) = \frac{100}{s^2/(0.01)^2 + 2 \times 0.7s/0.01 + 1} \quad (14)$$

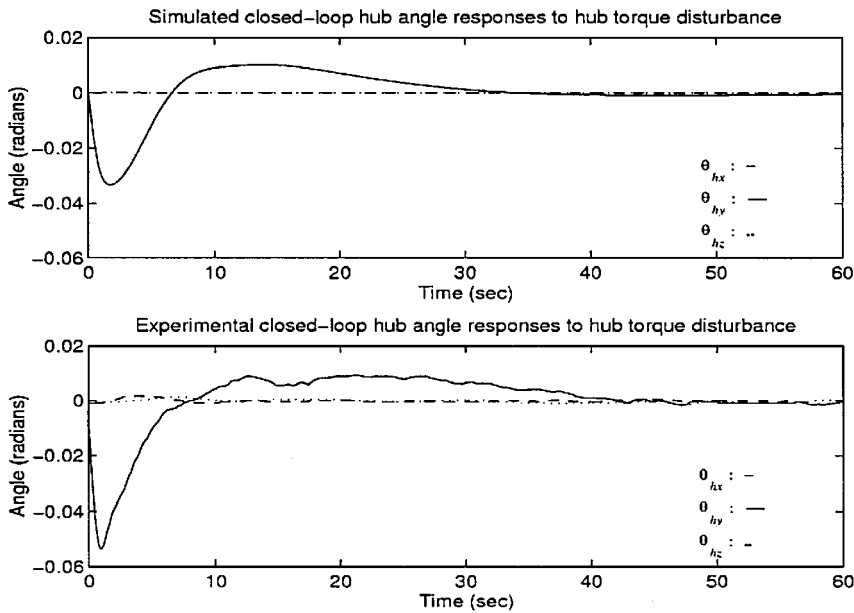$$r(s) = \frac{0.001s + 1.415}{2.33s + 1} \quad (15)$$

Fig. 8 Simulated and experimental closed-loop hub angle responses with K_{p1d}, D (13.5 N · m, 2 s, x).
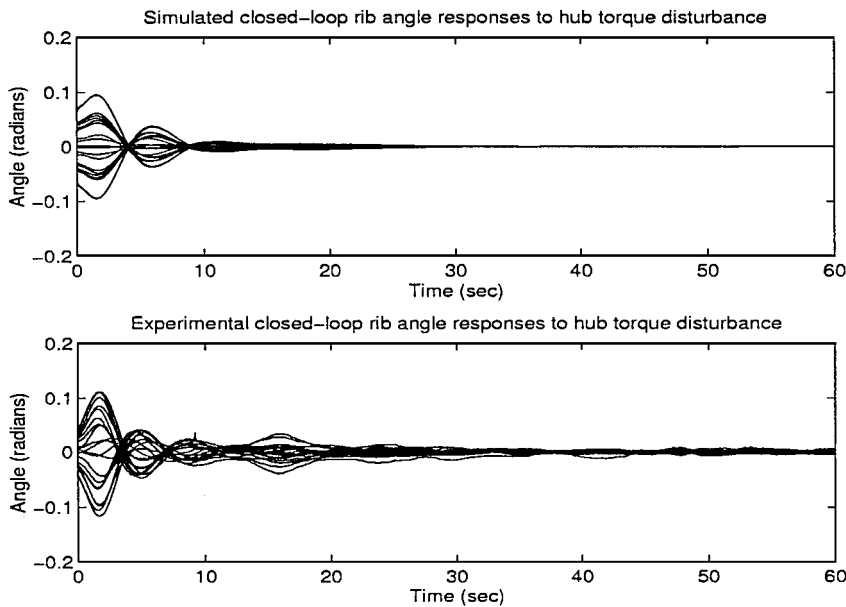

Fig. 9 Simulated and experimental closed-loop rib angle responses with K_{p1d}, D (13.5 N · m, 2 s, x).

A μ synthesis was carried out using μ-Tools functions[12] to implement the D–K iteration. Because the generalized plant model is 78th order, the D scales were restricted to be constant matrices to avoid an increase in the order of the controller. An additional benefit provided by constant D scales is robustness against linear time-varying and nonlinear perturbations (see Ref. 16 and the references therein). Thus, we have

$$D = \begin{bmatrix} dI & 0 \\ 0 & I \end{bmatrix}$$

due to the simple structure of Γ. One D–K iteration produced a stable, 78th-order controller K achieving $\sup_{\omega \in \mathbb{R}} \mu_\Gamma \{\mathcal{F}_L[P(j\omega), K(j\omega)]\} = 0.91$. A balanced truncation[17] of K yielded the 55th-order controller K_1, which basically did not affect the closed-loop plot of μ vs frequency. The least-damped closed-loop mode has a damping ratio of 0.38.

The norms of the nominal sensitivity $S_{dh}(j\omega)$, the worst-case sensitivity $S_{dhwc}(j\omega)$, and of five perturbed sensitivities $\{S_{dhpi}(j\omega)\}_{i=1}^5$ for five random sets of perturbations of the modal parameters of the plant model G within their limits are plotted in Fig. 6. The worst-case

sensitivity was obtained by perturbing the frequency response of the closed loop with the worst-case full uncertainty block, which can be computed using μ-Tools. All of these curves lie below $|w^{-1}(j\omega)|$ as expected, and furthermore, all five dotted curves corresponding to the perturbed sensitivities are very close to the nominal one. One can see that there is room between the perturbed sentivities and the worst-case one, which illustrates the conservativeness in the uncertainty model.

The 55th-order μ controller K_1 was rescaled to $K_{p1} = (d_{max}/\gamma)J_2^{-1}K_1$. Then K_{p1} was discretized at a sampling rate of 10 Hz using the bilinear transformation to get the controller K_{p1d}.

We used the standardized hub torque disturbance profile in Fig. 7 for all our test experiments and linear simulations. It can be applied by any of Daisy's three torque wheels individually or in any combination. The amplitude of the first torque pulse is A_d (in newtons), its duration is T seconds, and for this study it is applied around axis $\in \{x, y, z\}$.

In all of the experiments and simulations, the controller is switched on after the hub angle experiencing the largest deviation changes sign. For all of the plots, $t = 0$ corresponds to the instant at which the controller is turned on. The hub angle encoder
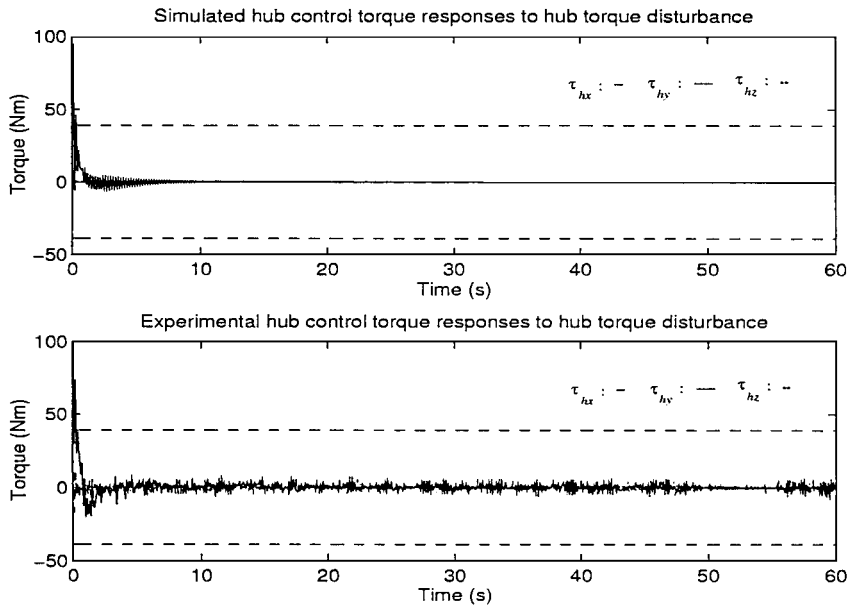

Fig. 10 Simulated and experimental computed hub control torques for K_{p1d}, D (13.5 N·m, 2 s, x).
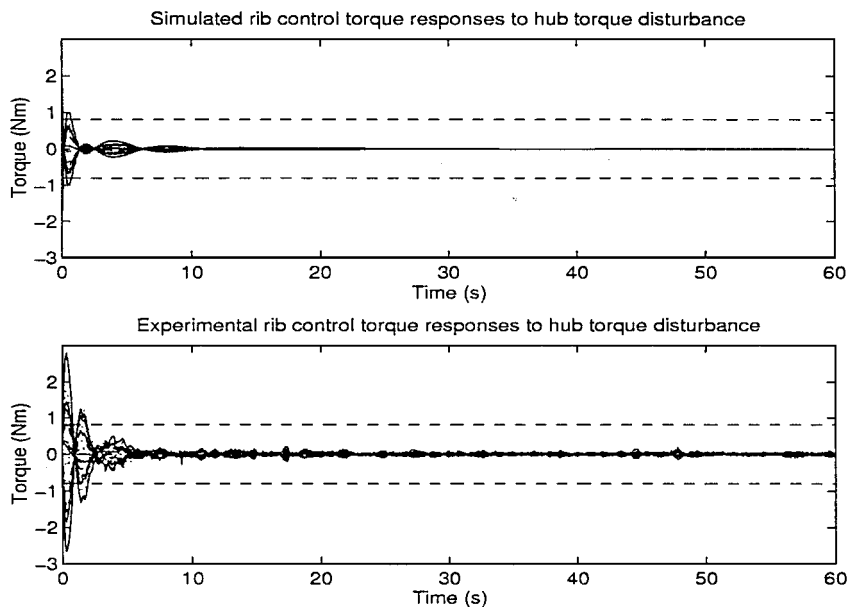

Fig. 11 Simulated and experimental computed rib control torques for K_{p1d}, D (13.5 N·m, 2 s, x).

measurements are accurate to within 1×10^{-4} rad. In the ideal case, the accuracy of DEOPS is 3.5×10^{-4} rad. The noise level was low, with an amplitude bound of 10^{-3} rad in both types of measurements. First, an x-axis hub torque disturbance D (13.5 N · m, 2 s, x) was applied to Daisy controlled by K_{p1d}. Simulated and experimental hub angles are shown in Fig. 8, and Fig. 9 shows the simulated and experimental rib angles. The latter are remarkably similar given the complexity of Daisy. The experimental and simulated hub responses are similar, although the experimental transient shows a larger peak. Moreover, the experimental settling time of θ_{hx} is longer than the simulated one.

The simulated and experimental computed control torques are shown in Fig. 10 for the hub and in Fig. 11 for the ribs. Both Figs. 10 and 11 indicate that the actuators saturated during the first few seconds (the dashed lines represent saturation limits). The next control experiments conducted with K_{p1d} involved torque disturbances around the y and z axes: D (13.5 N · m, 2 s, y) and D (13.5 N · m,

2 s, z). Results for the y-axis and z-axis experiments were similar to those to the x-axis experiment and are, therefore, not shown here (see Ref. 14).

B. Controller Design: Noncollocated Case

Earlier noncollocated control experiments on Daisy had shown that a more refined nominal model would be necessary for stability, with less uncertainty in the modal frequencies. An attempt was, thus, made to adjust the modal frequencies based on identification experiments (Table 1). These identification experiments consisted of recording step responses for all outputs and using the modal matrix to compute the step responses of the modal coordinates. The nominal modal frequencies and damping ratios were adjusted from these responses to obtain the refined model, and tighter uncertainty bounds were then estimated.

Our specifications are still robust stability and robust torque disturbance rejection, that is, $\|S_{dhp}(j\omega)\| \le |w^{-1}(j\omega)|$, $\forall \omega$, for all
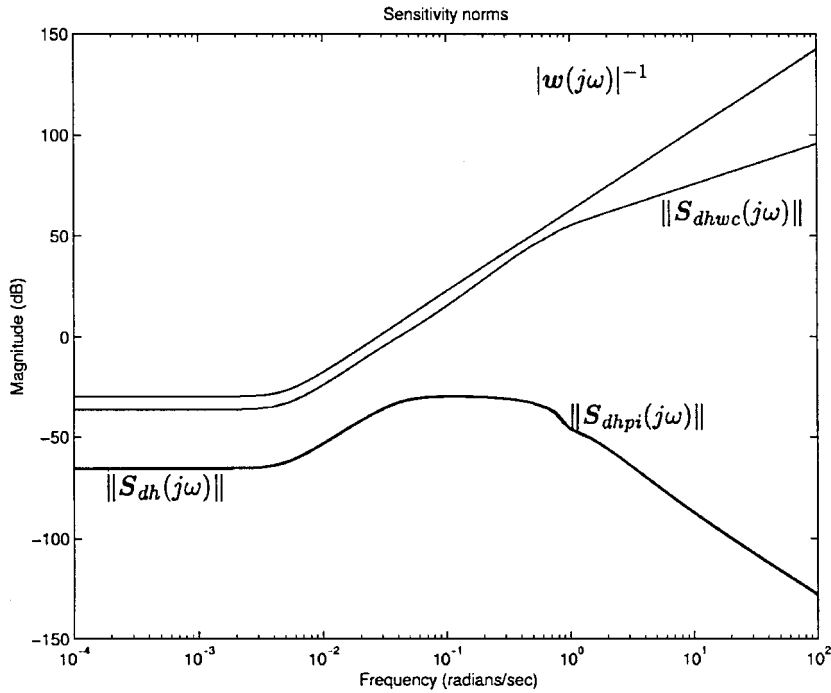

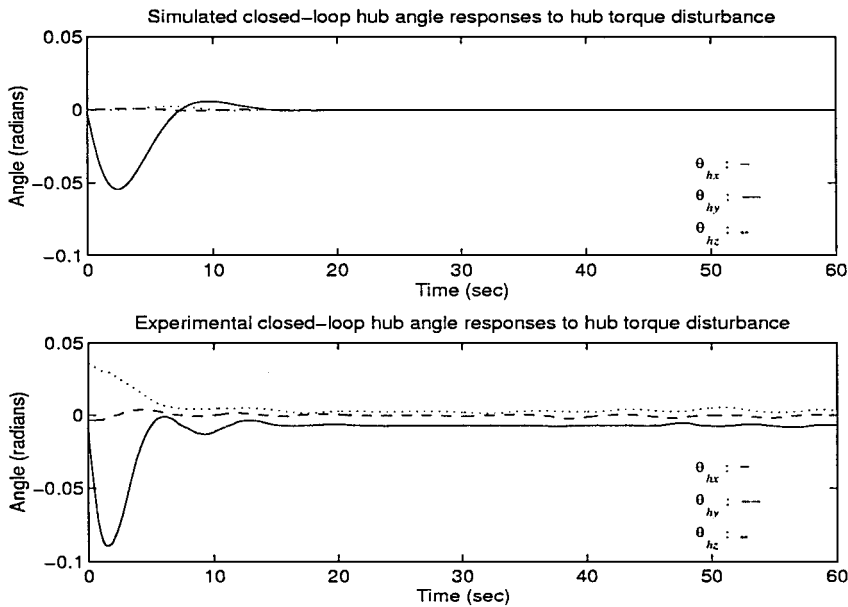Fig. 12   Norms of $S_{dh}(j\omega)$, $S_{dhwc}(j\omega)$, and $S_{dhp_i}(j\omega)$ for K_2.

Fig. 13   Simulated and experimental closed-loop hub angle responses with K_{p2d}, D (6.8 N · m, 2 s, x).

bounded perturbations of the modal parameters in Table 1 and all perturbations of the entries of B_1 within 5% of their nominal values. Note that the performance requirement has been relaxed here because the dc gain of w has been decreased to 30. This came about because of the tradeoff between nominal performance and performance robustness accommodating a reasonable amount of uncertainty. A few iterations of the design indicated that the chosen w led to a seemingly good tradeoff, with robustness to 5% uncertainty in the entries of B_1, 5% uncertainty in the modal frequencies, and 30% uncertainty in the damping ratios. Hence, this design could not quite meet the specifications, but it was close. The constants and weighting functions are

$$d_{\max} = 0.064, \qquad \gamma = 0.46$$

$$w(s) = \frac{30}{s^2/(0.005)^2 + 2 \times 0.7s/0.005 + 1} \qquad (16)$$

$$r(s) = \frac{0.01s + 1.415}{2.33s + 1} \qquad (17)$$

The noncollocated generalized plant model is 75th order. The D–K iteration was again restricted to constant D scales. One D–K iteration produced a stable, 75th-order controller K achieving $\sup_{\omega \in \mathbb{R}} \mu_\Gamma \{\mathcal{F}_L[P(j\omega), K(j\omega)]\} = 1.01$. A balanced realization of K was truncated to the 49-state controller K_2 without noticeably affecting μ vs frequency. The least-damped closed-loop mode has a damping ratio of 0.19.

The norms of the nominal sensitivity $S_{dh}(j\omega)$, the worst-case sensitivity $S_{dhwc}(j\omega)$ and of five perturbed sensitivities $\{S_{dhpi}(j\omega)\}_{i=1}^{5}$ for five random sets of perturbations of modal parameters (within their limits) in the plant model G, are plotted in Fig. 12. These five curves lie below $|w^{-1}(j\omega)|$ as expected, and furthermore, they are all very close to the nominal curve.

The 49th-order controller K_2 was rescaled to $K_{p2} = (d_{\max}/\gamma)J_2^{-1}K_2$, then discretized at a sampling rate of 10 Hz to get K_{p2d} using the bilinear transformation.

The responses to x-axis and y-axis hub torque disturbances were stable in the closed-loop experiments with K_{p2d}, but not the response to a z-axis disturbance. An x-axis hub torque disturbance D (6.8 N·m, 2 s, x) was applied to the system. Simulated and recorded hub and rib angles are shown in Figs. 13 and 14. The hub angle responses were stable, and the transients were satisfactory. The experimental settling time of θ_{hx} is close to the one obtained by simulation. The transients in the experimental rib angle responses are
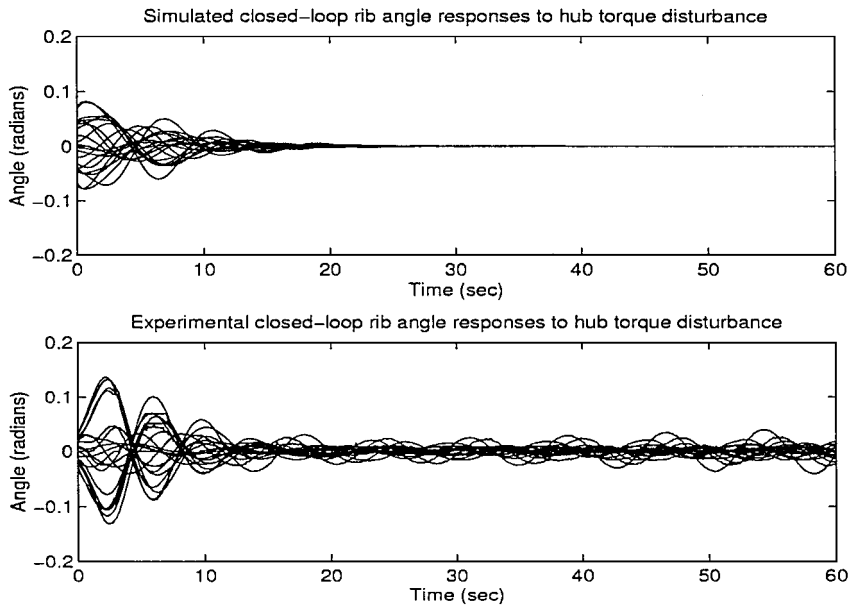

Fig. 14 Simulated and experimental closed-loop rib angle responses with K_{p2d}, D (6.8 N · m, 2 s, x).
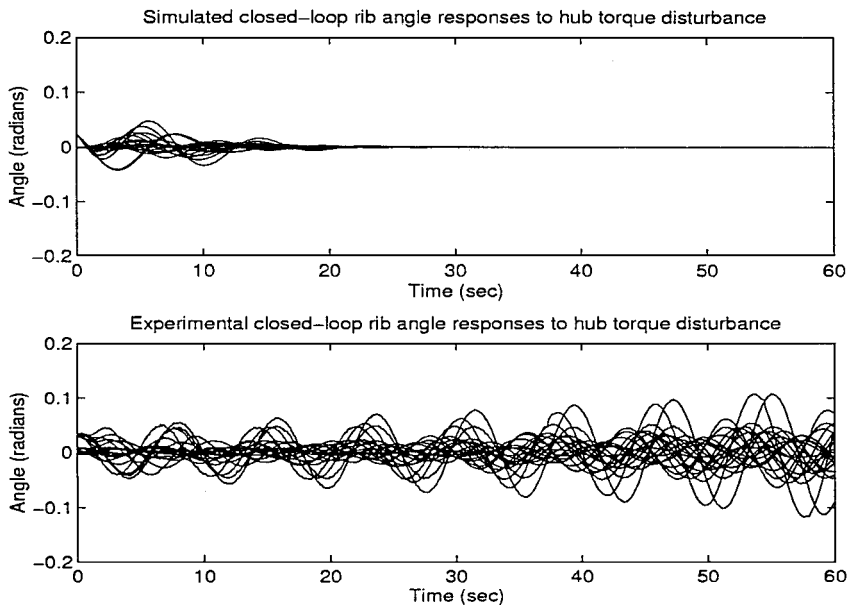

Fig. 15 Simulated and experimental closed-loop rib angle responses with K_{p2d}, D (6.8 N · m, 2 s, z).

seen to be a bit larger than in the simulation and lasted roughly twice as long. The simulated and experimental computed control torques remained within ± 10 N $\cdot$ m for the hub and ± 0.5 N $\cdot$ m for the ribs.

The next control experiments with K_{p2d} involved torque disturbances around the y axis and the z axis: D (6.8 N $\cdot$ m, 2 s, y) and D (6.8 N $\cdot$ m, 2 s, z). The hub and rib angle responses for the y-axis disturbance were similar to the responses obtained with the x-axis disturbance, and so they are not shown here (see Ref. 14). For the z-axis disturbance, rib angle responses are shown in Fig. 15. Clearly this run was unstable. Only 40 s of data could be recorded before rib angles went out of range, causing DEOPS to crash.

To summarize the results of the noncollocated design, the linear simulations showed very good nominal performance, whereas the design itself indicated performance robustness to reasonably large deviations in the modal parameters. A z-axis torque disturbance unequivocally destabilized Daisy, showing input-dependent stability properties of the closed-loop system. This suggests that thruster and other nonlinearities play a significant role in the noncollocated configuration.

V.   Experimental Results with $\mathcal{H}_\infty$ Controllers

This section briefly describes the design of $\mathcal{H}_\infty$ controllers for Daisy and presents some experimental results obtained with them. Performance comparisons are made using the results obtained with the μ controllers in the preceding section.

A collocated and a noncollocated $\mathcal{H}_\infty$ controller were designed and tested on Daisy. The results were presented in Ref. 3. These designs provided robust stability for all $\Delta_0 \in \mathcal{D}_r$, which implies robust stability to all variations in the modal parameters within their bounds. They also achieve nominal performance, that is, $\|S_{dhp}(j\omega)\| \le |w^{-1}(j\omega)|$ for $\Delta_0 \equiv 0$. The generalized plant used for these designs was identical to the one used for μ synthesis, except that it did not have the torque disturbance d as an input. It also had a real scalar $q > 0$ multiplying the performance weighting function W to ensure that $\|S_{dh}(j\omega)\| \le |w^{-1}(j\omega)|$ when

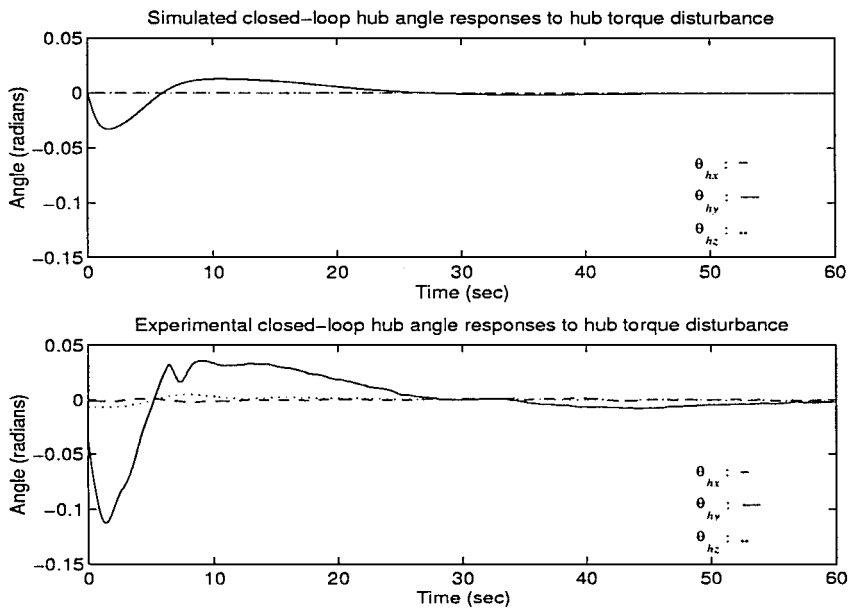$$\left\| w \mapsto \begin{bmatrix} z_1 \\ z_2 \end{bmatrix} \right\| \le 1$$

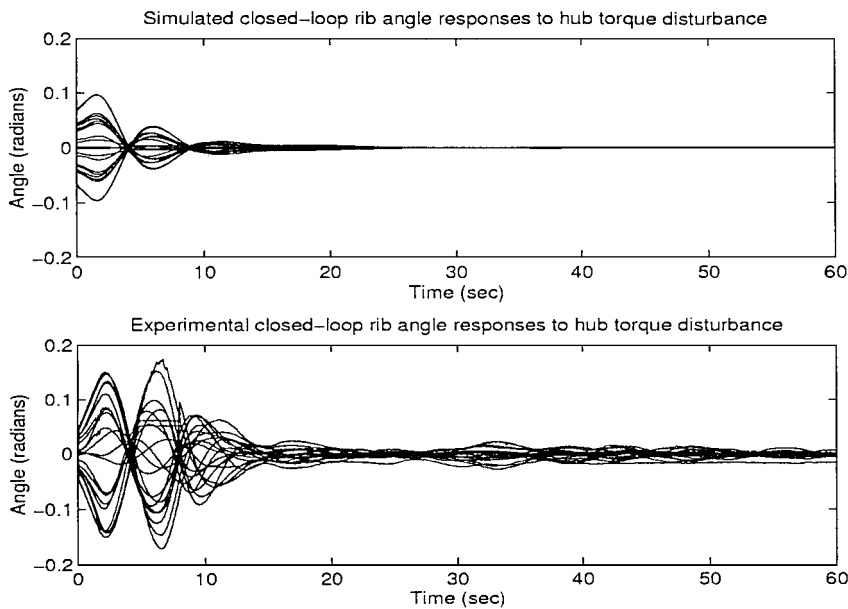**Fig. 16   Simulated and experimental closed-loop hub angle responses with K_{p3d}, D (13.5 N $\cdot$ m, 2 s, x).**

Fig. 17   Simulated and experimental closed-loop rib angle responses with K_{p3d}, D (13.5 N $\cdot$ m, 2 s, x).

For the $\mathcal{H}_\infty$ designs, robustness and nominal performance were lumped together in one full block in $\mathcal{RH}_\infty$ as opposed to two blocks as for the μ-synthesis designs.

Comparing the results obtained with the collocated $\mathcal{H}_\infty$ controller $\boldsymbol{K}_{p3d}$ (discretized at 10 Hz using the bilinear transformation) in Figs. 16 and 17, one can see that the μ controller performed better for an x-axis torque disturbance. This is especially evident for the rib responses. For the collocated μ controller, the experimental rib angles are close to the simulated ones, whereas with the $\mathcal{H}_\infty$ controller, the responses do not match as well. On the other hand, the two controllers produced very similar responses to a y-axis hub torque disturbance.[14]

Experimental results with the noncollocated $\mathcal{H}_\infty$ controller showed unstable responses for y-axis and z-axis hub torque disturbances and only a marginally stable response for an x-axis disturbance.[3,14]

VI. Conclusions

A μ-synthesis approach to the control of an LFSS experimental testbed called Daisy was described, and experimental results for collocated and noncollocated configurations of Daisy were given. Significant uncertainty in the modal parameters of Daisy in both configurations was handled with a coprime factorization technique introduced by the authors in a previous paper. Robust performance requirements were introduced by including a weighting function for torque disturbance to hub angles sensitivity shaping in the generalized plant. The designs produced stable discrete-time collocated and noncollocated controllers that were tested on Daisy.

The experimental responses to hub torque disturbances with the collocated μ controller were quite similar to the simulated responses obtained with the nominal model. The responses obtained with the collocated $\mathcal{H}_\infty$ controller were less similar to the nominal simulations. In the noncollocated case, stability was found to be input dependent with the μ controller doing slightly better than the $\mathcal{H}_\infty$ controller, with stable responses to x-axis and y-axis torque disturbances. The $\mathcal{H}_\infty$ controller produced a stable response only to an x-axis disturbance. Further research on LFSS modeling, identification, and stability analysis with nonlinearities will have to be carried out before we can hope to obtain better experimental results in noncollocated control of LFSS.

Acknowledgments

References

[1] Sparks, D. W., Jr., and Juang, J.-N., "Survey of Experiments and Experimental Facilities for Control of Flexible Structures," *Journal of Guidance, Control, and Dynamics*, Vol. 15, No. 4, 1992, pp. 801–816.

[2] Crocker, G. W., Hughes, P. C., and Hong, T., "Real-Time Computer Control of a Flexible Spacecraft Emulator," *IEEE Control Systems Magazine*, Vol. 10, No. 1, 1990, pp. 3–8.

[3] Boulet, B., Francis, B. A., Hughes, P. C., and Hong, T., "Uncertainty Modeling and Experiments in $\mathcal{H}_\infty$ Control of Large Flexible Space Structures," *IEEE Transactions on Control Systems Technology*, Vol. 5, No. 5, 1997, pp. 504–519.

[4] Lim, K. B., and Balas, G. J., "Line-of-Sight Control of the CSI Evolutionary Model: μ Control," *Proceedings of the American Control Conference*, IEEE Publications, Piscataway, NJ, 1992, pp. 1996–2000.

[5] Balas, G. J., and Doyle, J. C., "Robustness and Performance Tradeoffs in Control Design for Flexible Structures," *IEEE Transactions on Control Systems Technology*, Vol. 2, No. 4, 1994, pp. 352–361.

[6] Smith, R. S., Chu, C.-C., and Fanson, J. L., "The Design of $\mathcal{H}_\infty$ Controllers for an Experimental Non-Collocated Flexible Structure Problem," *IEEE Transactions on Control Systems Technology*, Vol. 2, No. 2, 1994, pp. 101–109.

[7] Lim, K. B., Maghami, P. G., and Joshi, S. M., "Comparison of Controller Designs for an Experimental Flexible Structure," *IEEE Control Systems Magazine*, Vol. 12, No. 3, 1992, pp. 108–118.

[8] Fan, M. K. H., Tits, A. L., and Doyle, J. C., "Robustness in the Presence of Mixed Parametric Uncertainty and Unmodeled Dynamics," *IEEE Transactions on Automatic Control*, Vol. AC-36, No. 1, 1991, pp. 25–38.

[9] How, J. P., Haddad, W. M., and Hall, S. R., "Robust Control Synthesis Examples with Real Parameter Uncertainty Using the Popov Criterion," *Proceedings of the American Control Conference*, IEEE Publications, Piscataway, NJ, 1993, pp. 1090–1095.

[10] How, J. P., Hall, S. R., and Haddad, W. M., "Robust Controllers for the Middeck Active Control Experiment Using Popov Controller Synthesis," *IEEE Transactions on Control Systems Technology*, Vol. 2, No. 2, 1994, pp. 73–87.

[11] Braatz, R. P., Young, P. M., Doyle, J. C., and Morari, M., "Computational Complexity of μ Calculation," *IEEE Transactions on Automatic Control*, Vol. AC-39, No. 5, 1994, pp. 1000–1002.

[12] Balas, G. J., Doyle, J. C., Glover, K., Packard, A., and Smith, R. S., "μ-Analysis and Synthesis Toolbox: User's Guide," Mathworks, Natick, MA, 1991.

[13] Laurin, D. G., Hughes, P. C., Guccione, R., and Cameron, I., "An Optical System for Shape Sensing of Flexible Space Structures," *Canadian Aeronautics and Space Journal*, Vol. 39, No. 1, 1993, pp. 45–51.

[14] Boulet, B., "Modeling and Robust Control of Large Flexible Space Structures," Ph.D. Dissertation, Dept. of Electrical and Computer Engineering, St. George Campus, Univ. of Toronto, Toronto, May 1996.

[15] Doyle, J. C., "Analysis of Feedback Systems with Structured Uncertainties," *IEEE Proceedings Part D*, Vol. 129, No. 6, 1982, pp. 242–250.

[16] Shamma, J. S., "Robust Stability with Time-Varying Uncertainty," *IEEE Transactions on Automatic Control*, Vol. 39, No. 4, 1994, pp. 714–724.

[17] Moore, B. C., "Principal Component Analysis in Linear Systems: Controllability, Observability, and Model Reduction," *IEEE Transactions on Automatic Control*, Vol. AC-26, No. 1, 1981, pp. 17–32.